Ceramics International xxx (xxxx) xxx–xxx

Contents lists available at ScienceDirect

Ceramics International

journal homepage: www.elsevier.com/locate/ceramint

Crystal structures and high microwave dielectric properties in Li^+/Ti^{4+} ions co-doped $Li_3Mg_2NbO_6$ ceramics

Ping Zhang[a,*], Kexin Sun[a], Xurui Mao[b,**], Mi Xiao[a], Zhentai Zheng[c]

[a] School of Electrical and Information Engineering, Key Laboratory of Advanced Ceramics and Machining Technology of Ministry of Education, Tianjin University, Tianjin, 300072, China

[b] State Key Laboratory on Integrated Optoelectronics, Institute of Semiconductors, Chinese Academy of Sciences, Beijing, 100083, China

[c] School of Materials Science and Engineering, Hebei University of Technology, Tianjin, 300130, China

ARTICLE INFO

Keywords:
Microwave dielectric properties
Li^+/Ti^{4+} ions co-doped
$Li_3Mg_2NbO_6$ ceramics

ABSTRACT

A series of novel $Li_{3+x}Mg_2Nb_{1-x}Ti_xO_6$ ($0.02 \le x \le 0.08$) ceramics with excellent microwave dielectric properties and relatively low sintering temperatures were synthesized via the solid-phase method. The correlations between sintering characteristics and microwave dielectric properties of the novel system were analyzed in detail. By (Li^+/Ti^{4+}) ions co-doped $Li_3Mg_2NbO_6$ ceramics, all compounds possessed a single phase with orthorhombic structure, pertaining to the space group Fddd (70). The change regulation of dielectric constant and $Q*f$ values was similar to density, which ascended to the maximum value first and then declined as the sintering temperature increased. Furthermore, the τ_f values constantly shifted to 0 ppm/°C with the content of complex ions (Li^+/Ti^{4+}) increasing. The best properties of $Li_{3.06}Mg_2Nb_{0.94}Ti_{0.06}O_6$ ceramics sintered at 1025 °C were $\varepsilon_r = 14.34$, $Q*f = 154{,}113$ GHz, and $\tau_f = -2.17$ ppm/°C.

1. Introduction

In recent decades, the proliferation of wireless communication technology has increased the demand for low-permittivity microwave dielectric ceramics in the form of dielectric substrates, ceramic package, and high-end microwave components [1–3]. To achieve high speed and stable transmission, these microwave dielectric ceramics ought to possess low loss (high $Q*f$) and near-zero temperature coefficient of resonate frequency [4,5]. Recently, many low-permittivity microwave dielectric materials have drawn researchers' attention, such as Li_2O–MgO–TiO_2, $LiMPO_4$ (M = Mg, Mn, Zn, Ni), Li_2AGeO_4 (A = Zn, Mg) et al. [6–10]. However, the relatively high sintering temperature or low $Q*f$ value hinders their development. Related studies have shown that $Li_3Mg_2NbO_6$ ceramics are of research value due to outstanding microwave dielectric properties and relatively low sintering temperature [11,12].

At present, the microwave dielectric properties of rock salt structured $Li_3Mg_2NbO_6$ ceramics have received extensive research attention. In 2009, the $Li_3Mg_2NbO_6$ compound as a new type microwave dielectric ceramic was first proposed by Yuan et al [13]. The properties of $Li_3Mg_2NbO_6$ ceramics were $\varepsilon_r = 16.8$, $Q*f = 79{,}643$ GHz, and $\tau_f = -27.2$ ppm/°C. In our past works, crystal structures and microwave dielectric properties of $Li_3Mg_2NbO_6$ ceramics were studied systematically when divalent and pentavalent ions (Ca^{2+}, Zn^{2+}, Mn^{2+}, Ni^{2+}, Sb^{5+}) were substituted for Mg^{2+} and Nb^{5+}, respectively. These study results indicated that ions substitution could greatly improve the properties of $Li_3Mg_2NbO_6$ ceramics [14–18]. In addition, Wu et al. [12] used complex chemical bond theory to explain the lattice energy, bond ionicity, and bond energy of $Li_3Mg_2NbO_6$ ceramics. Subsequently, they found that $Li_3(Mg_{0.98}Co_{0.02})_2NbO_6$ ceramics sintered at 1300 °C obtained superior performance of $\varepsilon_r = 15.22$, $Q*f = 127{,}600$ GHz, $\tau_f = -3.64$ ppm/°C [19]. Moreover, Zhao et al. [20] tried to synthesize $Li_3Mg_2NbO_6$ ceramics with nanopowders by using the high energy ball-milling method. In fact, there are still several feasible methods to optimize the performance of $Li_3Mg_2NbO_6$ ceramics.

Some researchers have suggested that the properties of lithium-based ceramics would be improved when aliovalent complex ions substituted for B-site ions. The $Q*f$ values of Li_2TiO_3 and Li_2MgTiO_4 dielectric ceramics were greatly improved by the substitution of $(Mg_{1/3}Nb_{2/3})^{4+}$ ions for Ti^{4+} ions [21,22]. Wu et al. [23] proposed that the $Li_2MgTi_{1-x}(Mg_{1/3}Ta_{2/3})_xO_4$ ($0 \le x \le 0.5$) ceramics with x = 0.4 obtained favorable $Q*f$ value of 184,000 GHz and the τ_f value was getting closer to zero with the increase of $(Mg_{1/3}Ta_{2/3})^{4+}$ ions. In the above studies, although ceramics possessed outstanding microwave dielectric

* Corresponding author.
** Corresponding author.
E-mail addresses: zptai@163.com (P. Zhang), maoxurui@semi.ac.cn (X. Mao).

https://doi.org/10.1016/j.ceramint.2019.12.036
Received 25 October 2019; Received in revised form 20 November 2019; Accepted 3 December 2019

properties, the sintering temperature (1250 °C, 1400 °C, and 1500 °C) was too high to be applied in practice. Thus, it is particularly important to find an experimental method that can not only boost performance but also reduce the sintering temperature of ceramics. In fact, raising the amount of Li^+ ions in lithium-based materials can enhance the $Q*f$ value and reduce the sintering temperature, due to suppressing the volatilization of lithium [24–26]. Meanwhile, the Ti^{4+} ions and Nb^{5+} ions have similar radii, and the Ti–O chemical bond is more stable than Nb–O due to short bond length [27]. Therefore, it is valuable to study the microwave dielectric properties and sintering behavior of Li^+/Ti^{4+} ions co-doped $Li_3Mg_2NbO_6$ ceramics.

In this work, a series of novel $Li_{3+x}Mg_2Nb_{1-x}Ti_xO_6$ ($0.02 \le x \le 0.08$) ceramics with excellent microwave dielectric properties and relatively low sintering temperature were synthesized via the solid-phase method. The sintering characteristics of $Li_{3+x}Mg_2Nb_{1-x}Ti_xO_6$ ($0.02 \le x \le 0.08$) ceramics were investigated in detail, and influence factors of microwave dielectric properties were analyzed systematically.

2. Experimental procedures

The $Li_{3+x}Mg_2Nb_{1-x}Ti_xO_6$ ($0.02 \le x \le 0.08$) ceramics were synthesized via the conventional solid-react method using analytical grade Li_2CO_3 (99%), MgO (99%), Nb_2O_5 (99%) and TiO_2 (99%). Weigh raw materials according to the stoichiometric ratio and ball mill the mixed raw materials for 8 h with deionized water and ZrO_2 balls in nylon jars. The obtained slurry was dried and screened through 40 mesh sieves. Then, the powers were calcined at 950 °C for 4 h in alumina crucibles, and the initial reaction powders were ball milled again. Subsequently, dried and sifted powders with 8 wt% petrolin were pressed into cylinders under a pressure of 5 MPa, the diameter and height of which were 10 mm and 5 mm, respectively. Finally, the cylinders were preheated at 550 °C for 3 h to exclude petrolin, and then sintered at temperature range 950°C–1050 °C for 4 h with a heating speed of 5 °C/min.

The X-ray diffraction (200kV/40 mA, 0.02°/step, Rigaku D/max 2550 PC, Tokyo, Japan) with Cu$K\alpha$ radiation were used to examine the structure characteristic and phase composition of $Li_{3+x}Mg_2Nb_{1-x}Ti_xO_6$ ($0.02 \le x \le 0.08$) ceramics. The surface microtopography of obtained ceramics was performed by one scanning electron microscopy (SEM, ZEISS MERLIN Compact, Germany). The grain size of surface microtopography was determined by Nano Measure software. The bulk density of specimens was calculated by Archimedes drainage method. The permittivity and unload $Q*f$ value were measured by Hakki and Coleman method with a network analyzer (9–11 GHz, N5234A, Agilent Co., America) and a cavity. The τ_f value was determined by Eq (1) in the temperature range from 25 °C to 85 °C:

$$\tau_f = \frac{f_2 - f_1}{f_1(T_2 - T_1)} \times 10^6 \quad (1)$$

where f_1 and f_2 represent the corresponding resonant frequency at the temperature of T_1 (25 °C) and T_2 (85 °C), respectively.

3. Results and discussions

The X-ray diffraction patterns of $Li_{3+x}Mg_2Nb_{1-x}Ti_xO_6$ ($0.02 \le x \le 0.08$) ceramics sintered at 1025 °C were demonstrated in Fig. 1. All diffraction peaks of specimens were matched with the orthorhombic structure $Li_3Mg_2NbO_6$ (PDF#86–0346) with no extra peaks in the observation range, which indicated that all $Li_{3+x}Mg_2Nb_{1-x}Ti_xO_6$ ceramics formed solid solutions in this work. Ti^{4+} substituted for Nb^{5+}, and excess Li^+ existed as interstitial atoms in the crystal. As the representative, the strongest diffraction peaks were plotted in the insertion diagram of Fig. 1. With the increase of complex ions (Li^+/Ti^{4+}) content, the peaks slightly displaced toward a higher 2θ angle, which implied that the unit cell volumes of $Li_{3+x}Mg_2Nb_{1-x}Ti_xO_6$ ceramics

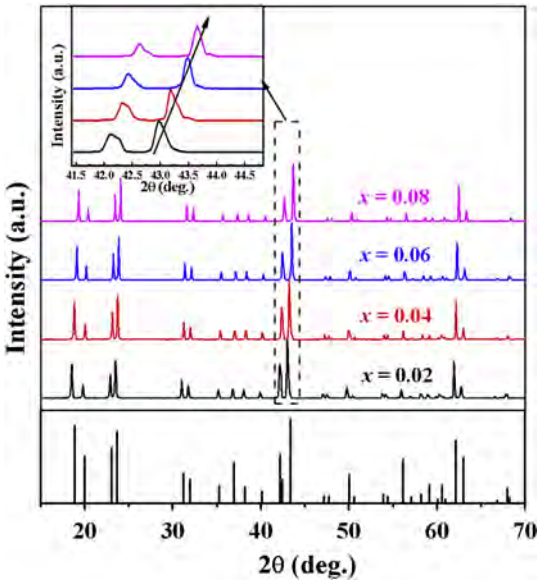

Fig. 1. The X-ray diffraction patterns of $Li_{3+x}Mg_2Nb_{1-x}Ti_xO_6$ ($0.02 \le x \le 0.08$) ceramics sintered at 1025 °C.

decreased due to the substitution of Ti^{4+} (0.605 Å) for Nb^{5+} (0.64 Å) in B site with the same coordination number (6) [27]. Previous studies revealed that the unit cell volumes of lithium-based ceramics increased with increasing excess Li content [5]. In this study, the influence of Ti^{4+} on the unit cell volume was much greater than that of Li^+, so the unit cell volumes of $Li_{3+x}Mg_2Nb_{1-x}Ti_xO_6$ ceramics decreased as complex ions (Li^+/Ti^{4+}) increased.

In order to understand the relationship between crystallographic structures and the content of complex ions (Li^+/Ti^{4+}) in detail, the X-ray diffraction patterns were refined by the Fullprof software using the Rietveld method. The X-ray diffraction patterns were continuously fitted with orthorhombic structured $Li_3Mg_2NbO_6$ (ICSD#86–0346) in the space group Fddd (70). Fig. 2 depicted refinement results of all compositions. The variance factors (R_p, R_{wp}) and the crystallographic structures including lattice parameters and unit cell volumes (V) were displayed in Table 1. There was a good fit between observed and calculated patterns because the values of R_p and R_{wp} were less than 15%, implying that the results of refinement were available. In addition, the unit cell volumes slightly decreased with the doping content, which exhibited the same conclusions as Fig. 1.

Fig. 3 displays surface microstructures of $Li_{3+x}Mg_2Nb_{1-x}Ti_xO_6$ ($0.02 \le x \le 0.08$) ceramics sintered at 1025 °C. It could be seen from Fig. 3 that all specimens had dense and homogeneous surface microstructures with precious few pores. In Fig. 3 (a)–(c), the grain size grew larger and tended to homogenization with complex ions (Li^+/Ti^{4+}) increasing. The average grain sizes of majority grain were ~8.12 μm, ~10.54 μm, and ~12.51 μm in turn. There were almost no pores in the microstructure of the specimen when x = 0.06. However, the grain size (average grain size of majority grain: ~7.90 μm) sharply decreased when x = 0.08 in Fig. 3(d), indicating that excessive complex ions (Li^+/Ti^{4+}) inhibited grain growth and seriously destroyed the microstructure of ceramics. In general, the grain boundaries would increase with decreasing grain size, leading the distribution of defects and impurities easy to concentrate on the grain boundaries [28]. Thus, some pores have appeared in Fig. 3 (d).

Fig. 4 presents the bulk density (ρ_{bulk}) and relative density (ρ_{th}) of $Li_{3+x}Mg_2Nb_{1-x}Ti_xO_6$ ($0.02 \le x \le 0.08$) ceramics as a function of complex ions (Li^+/Ti^{4+}) doping content and sintering temperatures. In the horizontal direction, the bulk density of $Li_{3+x}Mg_2Nb_{1-x}Ti_xO_6$ ceramics firstly rose to the maximum value at 1025 °C and then dropped sharply with the temperature increasing. In the longitudinal direction,

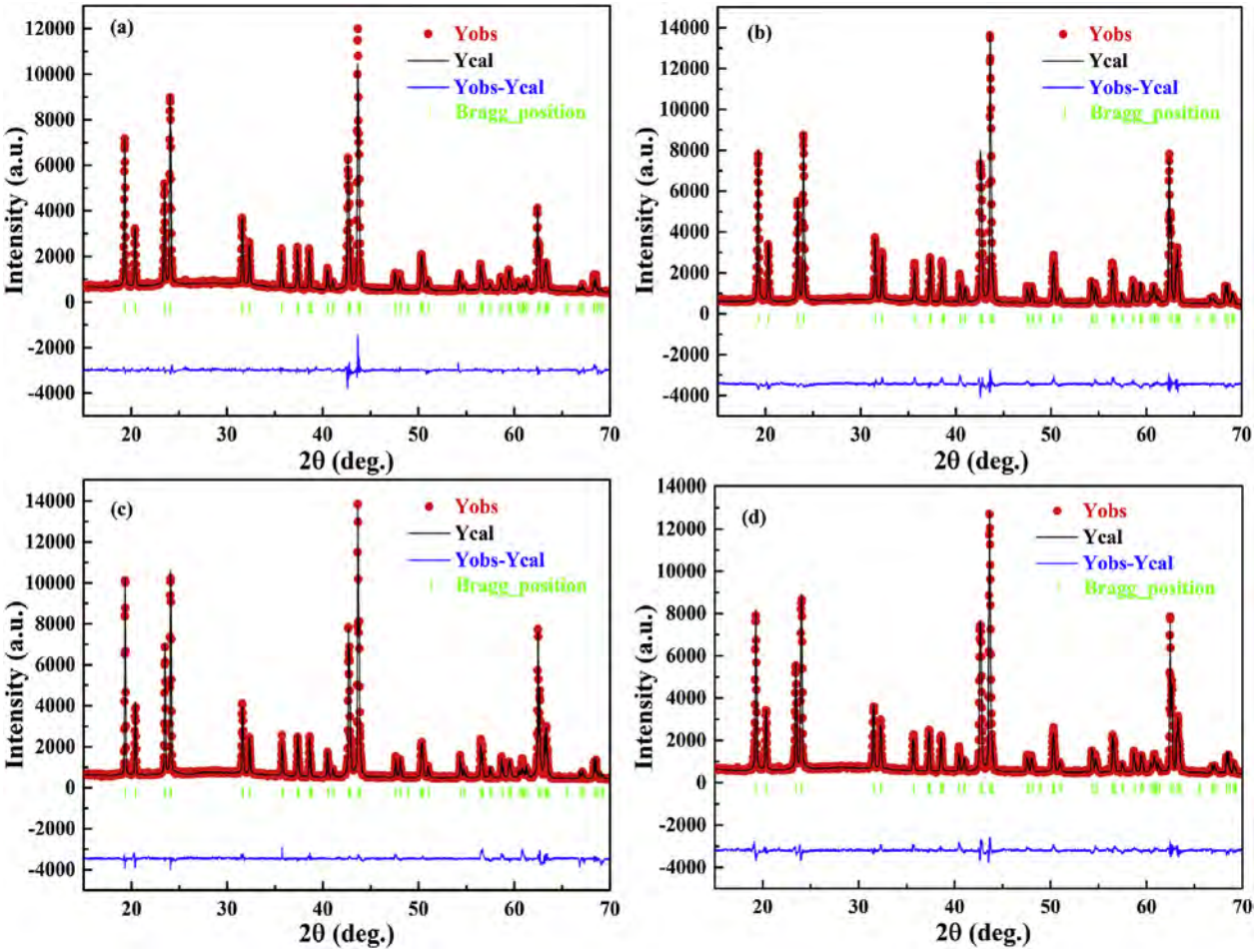

Fig. 2. Refinement results of $Li_{3+x}Mg_2Nb_{1-x}Ti_xO_6$ ($0.02 \le x \le 0.08$) ceramics sintered at 1025 °C: (a) x = 0.02, (b) x = 0.04, (c) x = 0.06, (d) x = 0.08.

Table 1
Reliability factors and crystallographic structures of $Li_{3+x}Mg_2Nb_{1-x}Ti_xO_6$ ($0.02 \le x \le 0.08$) ceramics sintered at 1025 °C.

x	R_p (%)	R_{wp} (%)	a	b	c	α = β = γ	V(Å)
0.02	11.4	12.0	5.9071	8.5581	17.7509	90°	897.3798
0.04	11.8	11.8	5.9027	8.5480	17.7437	90°	895.2700
0.06	10.5	13.9	5.9031	8.5436	17.7432	90°	894.8491
0.08	12.3	12.3	5.9031	8.5400	17.7429	90°	894.4520

the $Li_{3.06}Mg_2Nb_{0.94}Ti_{0.06}O_6$ ceramics behaved the best density regardless of sintered temperatures. Thus, the $Li_{3.06}Mg_2Nb_{0.94}Ti_{0.06}O_6$ ceramics sintered at 1025 °C were attained for the maximum bulk density ~3.45 g/cm^3. The variation of density was mainly related to the grain size and porosity in Fig. 3. The relative density of $Li_{3+x}Mg_2Nb_{1-x}Ti_xO_6$ ($0.02 \le x \le 0.08$) ceramics was computed by Eqs (2) and (3):

$$\rho_{th} = \frac{ZM}{VN_A} \tag{2}$$

$$\rho_{re} = \frac{\rho_{bulk}}{\rho_{th}} \times 100\% \tag{3}$$

where Z was the number of molecules in a single unit cell, M was the molecular mass, V is the unit cell volume, and N_A is the Archimedes constant. As shown in Fig. 4, the relative density and bulk density change trend was about the same. The sharp peak of relative density indicated that the effect of sintering temperature on density increased [29]. The relative density of $Li_{3+x}Mg_2Nb_{1-x}Ti_xO_6$ ceramics sintered at 1025 °C fluctuated from 91.08% to 98.53%, implying that the doping

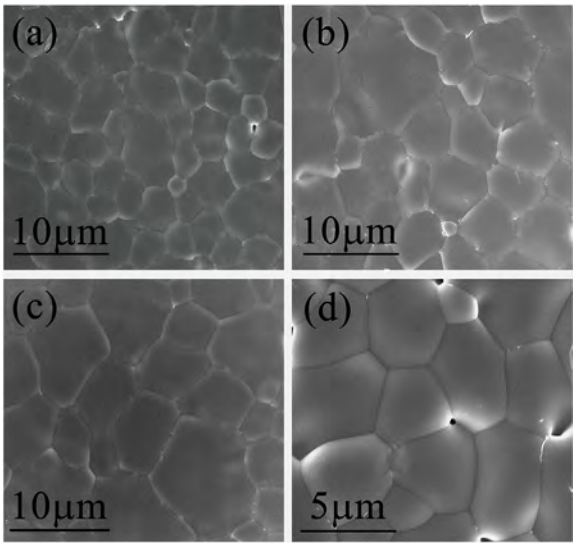

Fig. 3. The surface microstructures of $Li_{3+x}Mg_2Nb_{1-x}Ti_xO_6$ ($0.02 \le x \le 0.08$) ceramics sintered at 1025 °C: (a) x = 0.02, (b) x = 0.04, (c) x = 0.06, (d) x = 0.08.

content of complex ions (Li^+/Ti^{4+}) had a great influence on the relative density of specimens. When $x \le 0.06$, the Li^+ in complex ions compensated for the volatilization of lithium during the sintering process, increasing the density of ceramics. When $x > 0.06$, the density decreased because excessive complex ions (Li^+/Ti^{4+}) inhibited grain

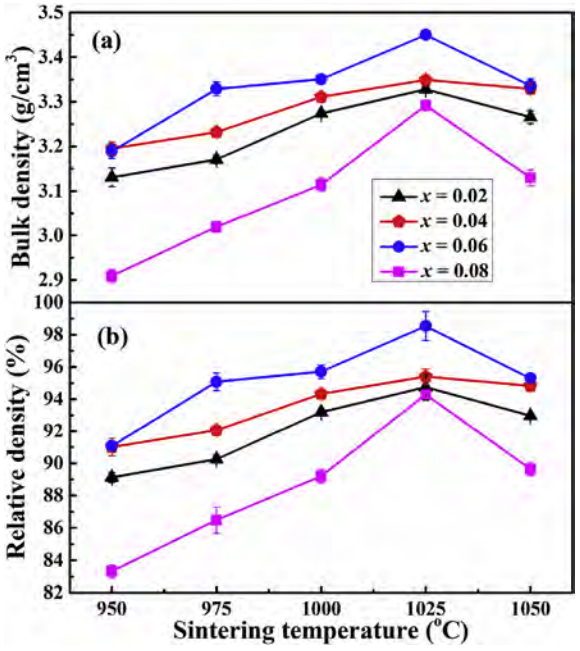

Fig. 4. (a) The bulk density and (b) relative density of $Li_{3+x}Mg_2Nb_{1-x}Ti_xO_6$ ($0.02 \le x \le 0.08$) ceramics as a function of complex ions (Li^+/Ti^{4+}) doping content and sintering temperatures.

growth and increased microscopic defects.

The dielectric constant (ε_r) of $Li_{3+x}Mg_2Nb_{1-x}Ti_xO_6$ ($0.02 \le x \le 0.08$) ceramics sintered at 950°C–1050 °C for 4 h was illustrated in Fig. 5. In general, the ε_r values of microwave ceramics is controlled by lattice structure, ionic polarizability, density, and second phase. In the above discussions (Fig. 1), the ceramics with a single phase had no structure change throughout the study. Thus, the ε_r of $Li_{3+x}Mg_2Nb_{1-x}Ti_xO_6$ ceramics was depended on ionic polarizability and density. As shown in Fig. 5, the trend of the curve between ε_r and sintering temperature was similar to that between density and sintering temperature (Figs. 4 and 5). The ε_r values first increased to the maximum at the optimum sintering temperature and then decreased, which was related to the grain size and porosity of ceramics microstructures. Moreover, it was easy to notice that the maximum ε_r value of each composition linearly increased from ~13.26 to ~14.49 with x value increased. To figure out the influence of ionic polarizability on ε_r, the

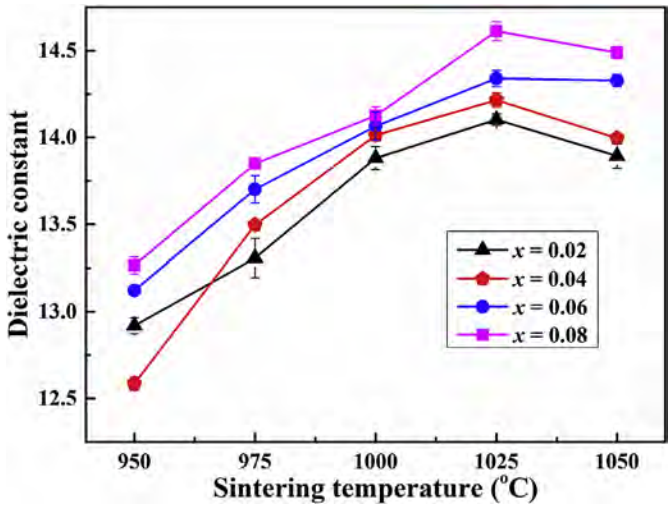

Fig. 5. The dielectric constant of $Li_{3+x}Mg_2Nb_{1-x}Ti_xO_6$ ($0.02 \le x \le 0.08$) ceramics sintered at 950°C–1050 °C.

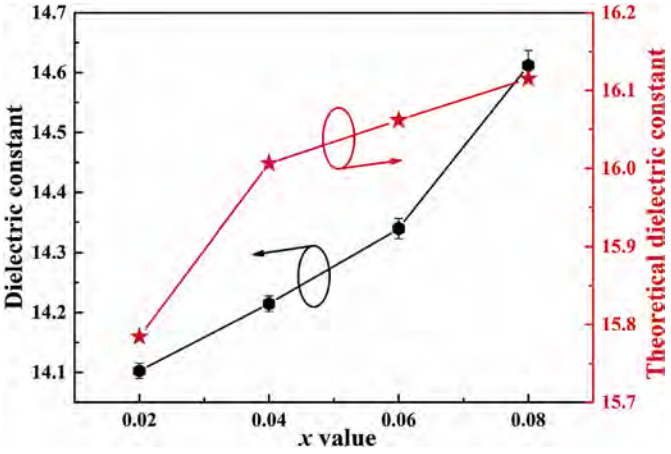

Fig. 6. The dielectric constant and theoretical dielectric constant of $Li_{3+x}Mg_2Nb_{1-x}Ti_xO_6$ ($0.02 \le x \le 0.08$) ceramics sintered at 1025 °C.

theoretical ionic polarizability (α_{theo}) of $Li_{3+x}Mg_2Nb_{1-x}Ti_xO_6$ ceramics was calculated through the additivity rule of constituent ionic polarizability suggested by Shannon [30]:

$$\alpha_{theo} = (3 + x)\alpha_{Li^+} + 2\alpha_{Mg^{2+}} + (1 - x)\alpha_{Nb^{5+}} + x\alpha_{Ti^{4+}} + 6\alpha_{O^{2-}} \quad (4)$$

while the theoretical dielectric constant (ε_{theo}) was measured using the Clausius-Mossotti equation as follow [31]:

$$\varepsilon_{theo} = \frac{3V_m + 8\pi\alpha_{theo}}{3V_m - 4\pi\alpha_{theo}} \quad (5)$$

where V_m was molar volume obtained from unit cell volumes (V) in Table 1. The ε_r and ε_{theo} of $Li_{3+x}Mg_2Nb_{1-x}Ti_xO_6$ ceramics sintered at 1025 °C were plotted in Fig. 6, and the positive discrepancy ($\triangle(\%) = |(\varepsilon_{theo} - \varepsilon_r)|/\varepsilon_r$) between ε_r and ε_{theo} was summarized in Table 2. Inspection from Fig. 6, the ε_r and ε_{theo} increased almost linearly with increasing x, which proved that ionic polarizability was the main factor of ε_r of $Li_{3+x}Mg_2Nb_{1-x}Ti_xO_6$ ceramics at the optimum sintering temperature. The polyhedrons in low symmetry structure were apt to distort, and then high polarizability "rattling" cations would appear in the center of distorted polyhedrons, which led the experimental dielectric constant to deviate from the dielectric constant calculated by the Clausius-Mossotti equation [31]. Accordingly, the low symmetry structure (orthorhombic) of $Li_{3+x}Mg_2Nb_{1-x}Ti_xO_6$ ceramics resulted in the deviation ($\triangle(\%)$) between ε_r and ε_{theo}.

Fig. 7 exhibits the quality factor ($Q*f$) of $Li_{3+x}Mg_2Nb_{1-x}Ti_xO_6$ ($0.02 \le x \le 0.08$) ceramics at a series of sintering temperatures. The maximum $Q*f$ values for each composition appeared at a sintering temperature of 1025 °C. At optimal sintering temperature, the $Q*f$ values increased from 128,929 GHz for $Li_{3.02}Mg_2Nb_{0.98}Ti_{0.02}O_6$ ceramic to 154,113 GHz for $Li_{3.06}Mg_2Nb_{0.94}Ti_{0.06}O_6$ ceramic, and then decreased to 117,813 GHz for $Li_{3.08}Mg_2Nb_{0.92}Ti_{0.08}O_6$ ceramic. In this work, the $Q*f$ values of specimens were higher than that of $Li_3Mg_2NbO_6$ ceramics studied by Yuan et al. [13], which was mainly due to two reasons. One was that excess Li^+ compensated for lithium volatilization at high sintering temperature, resulting in high density, uniform grain size and low porosity. The other was that the bond length of Ti–O was

Table 2
The detailed information of positive discrepancy ($\triangle(\%)$) between ε_r and ε_{theo} of $Li_{3+x}Mg_2Nb_{1-x}Ti_xO_6$ ($0.02 \le x \le 0.08$) ceramics sintered at 1025 °C.

x	α_{theo}	ε_{theo}	ε_r	$\triangle(\%)$
0.02	22.2732	15.7844	14.1027	11.92
0.04	22.2764	16.0063	14.2148	12.60
0.06	22.2796	16.0618	14.3398	12.01
0.08	22.2828	16.1153	14.6118	10.29

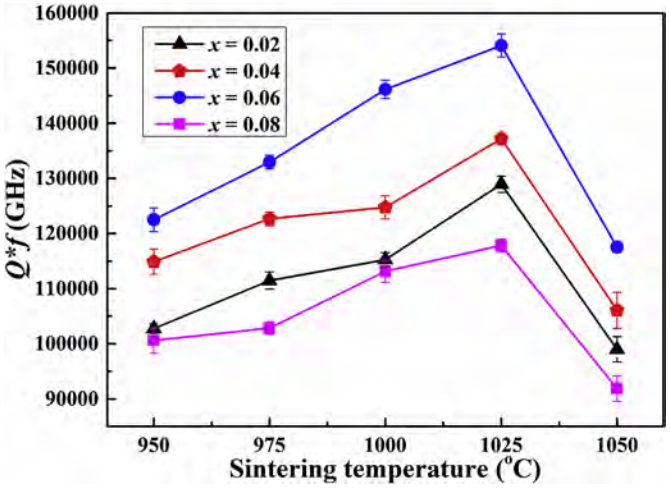

Fig. 7. The $Q*f$ values of $Li_{3+x}Mg_2Nb_{1-x}Ti_xO_6$ ($0.02 \le x \le 0.08$) ceramics sintered at various temperatures.

shorter than that of Nb–O, so the Ti–O bond was more stable than the Nb–O bond [27]. Besides, the optimal sintering temperature for $Q*f$ values of $Li_{3+x}Mg_2Nb_{1-x}Ti_xO_6$ ceramics was lower than that of $Li_3Mg_2NbO_6$ ceramics ($Li_{3+x}Mg_2Nb_{1-x}Ti_xO_6$ ceramics ~1025 °C, $Li_3Mg_2NbO_6$ ceramics ~1250 °C) [13].

In the microwave frequency range, the $Q*f$ values for dense materials with a single phase are generally influenced by intrinsic loss, such as the packing fraction. According to previous studies, the intrinsic loss of materials is negatively related to the intensity of internal lattice vibration. The higher the packing fraction, the lower the vibration intensity. Therefore, the $Q*f$ values increased [32]. The packing fraction (%) of $Li_{3+x}Mg_2Nb_{1-x}Ti_xO_6$ ceramics sintered at 1025 °C was calculated using Eq (6):

$$\text{Packing fraction} = \frac{\text{volume of the atoms in the cell}}{\text{volume of primitive unit cell}} = \frac{\text{volume of the atoms in the cell}}{\text{volume of unit cell}} \times Z \quad (6)$$

where Z has the same meaning as that in Eq (2). The calculated data of the packing fraction were tabulated as Table 3, and the correlation between $Q*f$ values and packing fraction of $Li_{3+x}Mg_2Nb_{1-x}Ti_xO_6$ ceramics was illustrated in Fig. 8. When $x \le 0.06$, the curves of packing fraction and $Q*f$ values exhibited an upward trend, indicating that $Q*f$ values were positively correlated with packing fraction. The increase of packing fraction led to the weakening of lattice vibration intensity, and the $Q*f$ values were improved. With further increasing the content of complex ions (Li^+/Ti^{4+}), the packing fraction of specimens continued to increase, while the $Q*f$ values decreased due to the lower density. In summary, the dominant factor of $Q*f$ values changed from intrinsic loss (packing fraction) to extrinsic loss (density, grain size and porosity) when the content of complex ions exceeded 0.06 in this work.

The τ_f value characterizes the shift of the resonant frequency with temperature. Generally, the τ_f value is dependent on the tilting of oxygen octahedron, which is mainly related to the bond energy [33]. Sanderson [34–36] reported that the bond energy is controlled by

Table 3
Ionic radius, Number of molecules in a single unit cell and Packing fraction of $Li_{3+x}Mg_2Nb_{1-x}Ti_xO_6$ ($0.02 \le x \le 0.08$) ceramics sintered at 1025 °C.

x	r_{Li}(Å)	r_{Mg}(Å)	$r_{Nb\text{-}Ti}$(Å)	r_O(Å)	Z	Packing fraction (%)
0.02	0.76	0.72	0.6394	1.36	8	65.07
0.04	0.76	0.72	0.6388	1.36	8	65.26
0.06	0.76	0.72	0.6382	1.36	8	65.32
0.08	0.76	0.72	0.6376	1.36	8	65.38

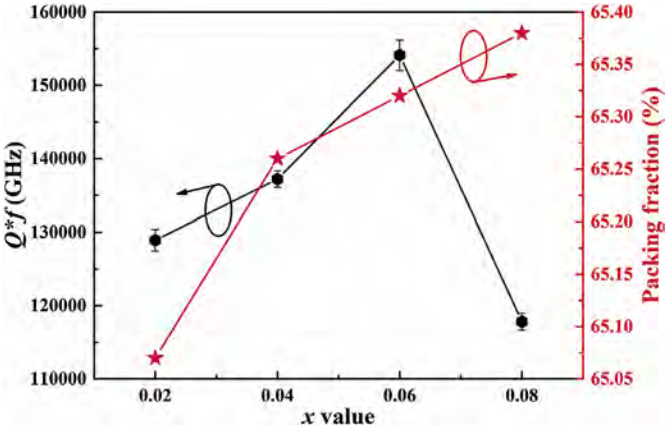

Fig. 8. The correlation between $Q*f$ values and packing fraction of $Li_{3+x}Mg_2Nb_{1-x}Ti_xO_6$ ceramics sintered at 1025 °C.

electronegativity and chemical bond. The bond energy (E) for a complex composition is calculated by Eqs (7) and (8):

$$E = \sum_{\mu} E_b^{\mu} \quad (7)$$

where E_b^{μ} is the bond energy of μ bond, which can be divided into ionicity energy E_i^{μ} and nonpolar covalence energy E_c^{μ} two parts:

$$E_b^{\mu} = t_i E_i^{\mu} + t_c E_c^{\mu} \quad (8)$$

the ionicity energy E_i^{μ} can be obtained from the constant (33,200) and bond length (d^{μ}/pm).

$$E_i^{\mu} = \frac{33200}{d^{\mu}} \quad (9)$$

the nonpolar covalence energy E_c^{μ} can be obtained from covalent radii r_c and homonuclear bond energy E_h.

$$E_c^{\mu} = \frac{(r_{cA} + r_{cB})}{d^{\mu}} (E_{hA-A} E_{hB-B})^{1/2} \quad (10)$$

in this work, r_{cLi} = 133 p.m., r_{cMg} = 139 p.m., r_{cNb} = 147 p.m., r_{cTi} = 136 p.m. and r_{cO} = 63 p.m.; $E_{hLi\text{-}Li}$ = 105 kJ mol^{-1}, $E_{hMg\text{-}Mg}$ = 11.3 kJ mol^{-1}, $E_{hNb\text{-}Nb}$ = 513 kJ mol^{-1}, $E_{hTi\text{-}Ti}$ = 117.6 kJ mol^{-1} and $E_{hO\text{-}O}$ = 498.36 kJ mol^{-1}, which were derived from handbook of chemical band energies [37]. In Eq (8), t_i and t_c are ionic and covalent blending coefficient, respectively. The relationship between t_i and t_c can be written as:

$$t_i + t_c = 1 \quad (11)$$

the t_i can be obtained from electronegativity (S_A and S_B) of each atom.

$$t_i = \left| \frac{(S_A - S_B)/\Delta S_B}{2} \right| \quad (12)$$

In this work, S_{Li} = 0.98, S_{Mg} = 1.31, S_{Nb} = 1.60, S_{Ti} = 1.54, S_O = 3.44 and $\triangle S_B$ = 3, which is the charge of complete electron.

According to the above formulas, the bond length and bond energy of $Li_{3+x}Mg_2Nb_{1-x}Ti_xO_6$ ($0.02 \le x \le 0.08$) ceramics sintered at 1025 °C were listed in Table 4. The τ_f values and bond energy as a function of the doped complex ions (Li^+/Ti^{4+}) content were presented in Fig. 9. The trend of τ_f values and bond energy were basically the same. With the increase of x value, τ_f values constantly shifted to a positive value and bond energy linearly increased, indicating that the $Li_{3+x}Mg_2Nb_{1-x}Ti_xO_6$ ceramics system tended to stability. In fact, the higher bond energy implied the shorter bond strength, which led to the restoring force of the system increasing. Therefore, the tilting of oxygen octahedrons decreased, and τ_f values increased.

Table 4
The bond length and bond energy of $Li_{3+x}Mg_2Nb_{1-x}Ti_xO_6$ ($0.02 \le x \le 0.08$) ceramics sintered at 1025 °C.

Bond type	Bond length (*d*) and bong energy (*E*)							
	x = 0.02		x = 0.04		x = 0.06		x = 0.08	
	d	E	d	E	d	E	d	E
Nb/Ti–O1	2.083	545.741	2.064	557.030	2.083	548.871	2.161	534.998
Nb/Ti–O2	2.068	549.700	2.093	549.312	2.109	542.087	2.154	536.639
Li1–O1	2.065	405.872	2.041	409.541	2.047	408.894	1.994	418.683
Li1–$O2^1$	2.182	384.109	2.175	384.328	2.170	385.770	2.194	380.586
Li1–$O2^2$	2.139	391.830	2.123	393.742	2.199	380.630	2.208	378.104
Li2–O1	2.186	383.488	2.152	388.511	2.102	398.288	2.065	404.288
Li2–$O2^1$	2.094	400.251	2.102	397.675	2.105	397.716	2.095	398.537
Li2–$O2^2$	2.018	415.325	2.027	412.389	2.060	406.313	2.053	406.651
Li3–O1	2.187	383.231	2.21	378.241	2.188	282.391	2.118	394.171
Li3–O2	2.066	405.675	2.106	396.920	2.024	413.540	2.074	402.629
Mg1–O1	2.065	286.036	2.041	289.385	2.047	288.551	1.994	296.221
Mg1–$O2^1$	2.182	270.699	2.175	271.570	2.170	272.233	2.194	269.267
Mg1–$O2^2$	2.139	276.140	2.123	278.221	2.199	268.606	2.208	267.511
Mg2–O1	2.186	270.261	2.152	274.525	2.102	281.067	2.065	286.036
Mg2–$O2^1$	2.094	282.075	2.102	281.001	2.105	280.663	2.095	281.967
Mg2–$O2^2$	2.018	292.698	2.027	291.398	2.060	286.730	2.053	287.708
Mg3–O1	2.187	270.080	2.21	267.269	2.188	269.849	2.118	278.878
Mg3–O2	2.066	285.897	2.106	280.467	2.024	291.830	2.074	284.862
TE[a]		6499.108		6501.528		6504.029		6507.736

[a] The **TE** was the total bond energy.

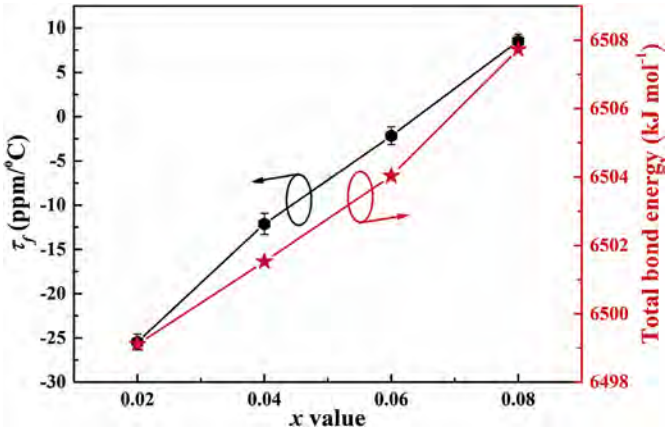

Fig. 9. The τ_f values and bond energy of $Li_{3+x}Mg_2Nb_{1-x}Ti_xO_6$ ($0.02 \le x \le 0.08$) ceramics sintered at 1025 °C as a function of the doped complex ions (Li^+/Ti^{4+}) content.

4. Conclusions

The $Li_{3+x}Mg_2Nb_{1-x}Ti_xO_6$ ($0.02 \le x \le 0.08$) system formed by Li^+/Ti^{4+} co-doped $Li_3Mg_2NbO_6$ ceramics were succeeded in synthesizing via the traditional solid-state reaction method. In this work, all compositions with a single phase formed solid solutions and showed dense microstructures. The change regulation of dielectric constant and $Q*f$ values was similar to that of density. The dielectric constant and τ_f values of $Li_{3+x}Mg_2Nb_{1-x}Ti_xO_6$ ceramics sintered at 1025 °C monotonously increased with increasing x, while the $Q*f$ values ascended to the maximum with x = 0.06 and then descended. In addition, this study found that the microwave dielectric properties of $Li_{3+x}Mg_2Nb_{1-x}Ti_xO_6$ ceramics were closely related to the lattice structure. The comprehensive performance of $Li_{3+x}Mg_2Nb_{1-x}Ti_xO_6$ ceramics superior to most other ceramic systems, such as $Li_2MgTi_{1-x}(Mg_{1/3}Ta_{2/3})_xO_4$, $Li_2MgTi_{1-x}(Mg_{1/3}Nb_{2/3})_xO_4$, $Li_3Mg_2NbO_6$ based ceramics, and so on. The excellent properties were achieved at the composition with x = 0.06: ε_r = 14.34, $Q*f$ = 154,113 GHz, τ_f = −2.17 ppm/°C.

Declaration of competing interest

There is no conflict of interest when submitting this manuscript, and the manuscript is approved by all authors for publication. On behalf of all the authors, I stated that the work described in this manuscript was original research, was not published before, and was not considered to be published in whole or in part elsewhere.

We declare that we do not have any commercial or associative interest that represents a conflict of interest in connection with the manuscript submitted.

Acknowledgments

This work was supported by Major Projects of Science and Technology in Tianjin (No. 18ZXJMTG00020), the National Natural Science Foundation of China (No. 61671323) and the Natural Science Foundation of Hebei Province, China (No. E2017202011).

References

[1] J. Guo, A.L. Baker, H. Guo, M. Lanagan, C.A. Randall, Cold sintering process: a new era for ceramic packaging and microwave device development, J. Am. Ceram. Soc. 100 (2017) 669–677.
[2] I.M. Reaney, D. Iddles, Microwave dielectric ceramics for resonators and filters in mobile phone networks, J. Am. Ceram. Soc. 89 (2006) 2063–2072.
[3] Y. Wang, S.B. Zhang, T.L. Tang, W.S. Xia, L.W. Shi, Investigation on microwave dielectric properties of new low-loss $CoZrTa_2O_8$ ceramics, Mater. Lett. 231 (2018) 1–4.
[4] T.A. Vanderah, Talking ceramics, Science 298 (2002) 1182–1184.
[5] Y. Tian, Y. Tang, K. Xiao, C. Li, L. Duan, L. Fang, Crystal structure, Raman spectroscopy and microwave dielectric properties of $Li_{1+x}ZnNbO_4$ ($0 \le x \le 0.05$) ceramics, J. Alloy. Comp. 777 (2019) 1–7.
[6] Y.D. Zhang, D. Zhou, Pseudo phase diagram and microwave dielectric properties of Li_2O-MgO-TiO_2 ternary system, J. Am. Ceram. Soc. 99 (2016) 3643–3650.
[7] H.F. Zhou, X.H. Tan, J. Huang, X.L. Chen, Sintering behavior, phase evolution and microwave dielectric properties of thermally stable Li_2O-$_3$MgO-mTiO_2 ceramics ($1 \le m \le 6$), Ceram. Int. 43 (2017) 3688–3692.
[8] D. Thomas, M.T. Sebastian, Temperature-compensated $LiMgPO_4$: a new glass-free low-temperature cofired ceramic, J. Am. Ceram. Soc. 93 (2010) 3828–3831.
[9] P. Zhang, S. Wu, M. Xiao, The microwave dielectric properties and crystal structure of low temperature sintering $LiNiPO_4$ ceramics, J. Eur. Ceram. Soc. 38 (2018) 4433–4439.
[10] C.C. Li, H.C. Xiang, M.Y. Xu, Y. Tang, L. Fang, Li_2AGeO_4 (A = Zn, Mg): two novel low permittivity microwave dielectric ceramics with olivine structure, J. Eur. Ceram. Soc. 38 (2018) 1524–1528.
[11] M. Castellanos, J.A. Gard, A.R. West, Crystal data for a new family of phases,

$Li_3Mg_2XO_6$: X = Nb, Ta, Sb, J. Appl. Crystallogr. 15 (1982) 116–119.
[12] H.T. Wu, E.S. Kim, Characterization of low loss microwave dielectric materials $Li_3Mg_2NbO_6$ based on the chemical bond theory, J. Alloy. Comp. 669 (2016) 134–140.
[13] L.L. Yuan, J.J. Bian, Microwave dielectric properties of the lithium containing compounds with rock salt structure, Ferroelectrics 387 (2009) 123–129.
[14] Y.G. Zhao, P. Zhang, Microstructure and microwave dielectric properties of low loss materials $Li_3(Mg_{0.95}A_{0.05})_2NbO_6$ (A = Ca^{2+}, Ni^{2+}, Zn^{2+}, Mn^{2+}) with rock-salt structure, J. Alloy. Compd 658 (2016) 744–748.
[15] P. Zhang, L. Liu, M. Xiao, Y.G. Zhao, A novel temperature stable and high *Q* microwave dielectric ceramic in $Li_3(Mg_{1-x}Mn_x)_2NbO_6$ system, J. Mater. Sci. Mater. Electron. 28 (2017) 12220–12225.
[16] P. Zhang, L. Liu, M. Xiao, Microwave dielectric properties of high *Q* and temperature stable $Li_3(Mg_{1-x}Ni_x)_2NbO_6$ ceramics, J. Mater. Sci. Mater. Electron. 29 (2018) 5057–5063.
[17] P. Zhang, K.X. Sun, L. Liu, M. Xiao, A novel low loss and low temperature sintering $Li_3(Mg_{1-x}Ca_x)_2NbO_6$ microwave dielectric ceramics by doping LiF additives, J. Alloy. Comp. 765 (2018) 209–217.
[18] P. Zhang, X.S. Wu, M. Xiao, Effect of Sb^{5+} ion substitution for Nb^{5+} on crystal structure and microwave dielectric properties for $Li_3Mg_2NbO_6$ ceramics, J. Alloy. Comp. 766 (2018) 498–505.
[19] C.F. Xing, J.X. Bi, H.T. Wu, Effect of Co-substitution on microwave dielectric properties of $Li_3(Mg_{1-x}Co_x)_2NbO_6$ ($0.00 \le x \le 0.10$) ceramics, J. Alloy. Comp. 719 (2017) 58–62.
[20] L.P. Zhao, P. Liu, G.Q. Sun, Z.F. Fu, Nanopowders preparation and dielectric properties of low-fired $Li_3Mg_2NbO_6$ ceramics, J. Mater. Sci. Mater. Electron. 29 (2018) 5873–5877.
[21] J.J. Bian, X.H. Zhang, Structural evolution, grain growth kinetics and microwave dielectric properties of $Li_2Ti_{1-x}(Mg_{1/3}Nb_{2/3})_xO_3$, J. Eur. Ceram. Soc. 38 (2018) 599–604.
[22] C.H. Yang, H.T. Wu, Phase composition, Raman spectra, infrared spectra and dielectric properties of $Li_2MgTi_{1-x}(Mg_{1/3}Nb_{2/3})_xO_4$ ceramics at microwave frequency, Ceram. Int. 44 (2018) 9255–9262.
[23] C.H. Yang, Q.Q. Liu, J.X. Bi, W.H. Tao, H.T. Wu, Effects of $(Mg_{1/3}Ta_{2/3})$-substitution for Ti-site on the microwave dielectric properties of Li_2MgTiO_4 ceramics, Ceram. Int. 44 (2018) 5982–5987.
[24] J.J. Bian, Y.F. Dong, Sintering behavior, microstructure and microwave dielectric properties of $Li_{2+x}TiO_3$ ($0 \le x \le 0.2$), Mater. Sci. Eng. B 176 (2011) 147–151.
[25] Y. Ding, J.J. Bian, Structural evolution, sintering behavior and microwave dielectric properties of $(1-x)Li_2TiO_3 + xLiF$ ceramics, Mater. Res. Bull. 48 (2013) 2776–2781.
[26] J. Song, J. Zhang, R. Zuo, Ultrahigh *Q* values and atmosphere-controlled sintering of $Li_{2(1+x)}Mg_3ZrO_6$ microwave dielectric ceramics, Ceram. Int. 43 (2017) 2246–2251.
[27] R.D. Shannon, Revised effective ionic radii and systematic studies of interatomic distances in halides and chalcogenides, Acta Crystallogr. 32 (1976) 751–767.
[28] S. Kucheiko, J.W. Choi, H.J. Kim, H.J. Jung, Microwave dielectric properties of $CaTiO_3$-$Ca(Al_{1/2}Ta_{1/2})O_3$ ceramics, J. Am. Ceram. Soc. 79 (1996) 2739–2743.
[29] X.Q. Song, W.Z. Lu, X.C. Wang, X.H. Wang, G.F. Fan, R. Muhammad, W. Lei, Sintering behaviour and microwave dielectric properties of $BaAl_{2-2x}(ZnSi)_xSi_2O_8$ ceramics, J. Eur. Ceram. Soc. 38 (2018) 1529–1534.
[30] R.D. Shannon, G.R. Rossman, Dielectric constants of silicate garnets and the oxide additivity rule, Am. Mineral. 77 (1992) 94–100.
[31] R.D. Shannon, Dielectric polarizabilities of ions in oxides and fluorides, J. Appl. Phys. 73 (1993) 348–366.
[32] E.S. Kim, B.S. Chun, R. Freer, R.J. Cernik, Effects of packing fraction and bond valence on microwave dielectric properties of $A^{2+}B^{6+}O_4$ (A^{2+}: Ca, Pb, Ba; B^{6+}: Mo, W) ceramics, J. Eur. Ceram. Soc. 30 (2010) 1731–1736.
[33] E.S. Kim, B.S. Chun, K.H. Yoon, Dielectric properties of $[Ca_{1-x}(Li_{1/2}Nd_{1/2})_x]_{1-y}Zn_yTiO_3$ ceramics at microwave frequencies, Mater. Sci. Eng. B 99 (2003) 93–97.
[34] R.T. Sandderson, Multiple and single bond energies in inorganic molecules, Inorg. Nucl. Chem. 30 (1968) 375–393.
[35] R.T. Sandderson, Chemical Bonds and Bond Energy, Academic Press, New York, 1971.
[36] R.T. Sandderson, Electronegativity and bond energy, J. Am. Chem. Soc. 105 (1983) 2259–2261.
[37] Y.R. Luo, Comprehensive Handbook of Chemical Bond Energies, CRC Press, 2007.